Earth and Space Science

RESEARCH LETTER
10.1029/2021EA001729

**Special Section:**
The Ice, Cloud and land Elevation Satellite-2 (ICESat-2) on-orbit performance, data discoveries and early science

# Enabling Value Added Scientific Applications of ICESat-2 Data With Effective Removal of Afterpulses

**Xiaomei Lu[1,2], Yongxiang Hu[2], Yuekui Yang[3], Mark Vaughan[2], Stephen Palm[1,3], Charles Trepte[2], Ali Omar[2], Patricia Lucker[1,2], and Rosemary Baize[2]**

[1]Science Systems and Applications, Inc., Hampton, VA, USA, [2]NASA Langley Research Center, Hampton, VA, USA, [3]NASA Goddard Space Flight Center, Greenbelt, MD, USA

**Key Points:**

- The effects of after-pulsing by the Advanced Topographic Laser Altimeter System (ATLAS) aboard the ICESat-2 satellite are described
- The transient response of the ATLAS receiver is characterized over different measurement regimes
- The potential impacts of these detector artifacts on ICESat-2 science studies are discussed

**Supporting Information:**

Supporting Information may be found in the online version of this article.

**Correspondence to:**

X. Lu and Y. Hu,
xiaomei.lu@nasa.gov;
yongxiang.hu-1@nasa.gov

**Citation:**

Lu, X., Hu, Y., Yang, Y., Vaughan, M., Palm, S., Trepte, C., et al. (2021). Enabling value added scientific applications of ICESat-2 data with effective removal of afterpulses. *Earth and Space Science*, *8*, e2021EA001729. https://doi.org/10.1029/2021EA001729

Received 28 FEB 2021
Accepted 17 APR 2021



**Abstract** The Advanced Topographic Laser Altimeter System (ATLAS) aboard the Ice, Cloud, and land Elevation Satellite-2 (ICESat-2) has been making very high resolution measurements of the Earth's surface elevation since October 2018. ATLAS uses photomultiplier tubes (PMTs) as detectors in photon counting mode, so that a single photon reflected back to the receiver triggers a detection within the ICESat-2 data acquisition system. However, one characteristic of ICESat-2 detected photons is the possible presence of afterpulses, defined as small amplitude pulses occurring after the primary signal pulse due to photon arrival. The disadvantage of these afterpulses is that they often confound the accurate measurements of low level signals following a large amplitude of signal and can degrade energy resolution and cause errors in pulse counting applications. This paper discusses and summarizes the after-pulsing effects exhibited by the ATLAS PMTs based on on-orbit measurements over different seasons and geographic regions. The potential impacts of these after-pulsing effects on altimetry and ocean subsurface retrievals are discussed.

**Plain Language Summary** After-pulsing effects occurring in the ICESat-2 Advanced Topographic Laser Altimeter System (ATLAS) are characterized from the on-orbit measurements acquired over different surface types. Multiple echoes due to after-pulsing effects in the ATLAS photomultiplier tubes (PMTs) are clearly seen below the Earth's surface where the signal should be totally attenuated. The afterpulses captured from on-orbit measurements are caused by three different reasons: (1) the effects of the dead-time circuit (~3 ns) due to PMT saturation; (2) the effects of optical reflections within the ATLAS receiver optical components; (3) PMT afterpulses. The echoes separated by ~0.45 m are attributed to the effect of the dead-time circuit (~3 ns) due to PMT saturation. The echoes at ~2.3 and ~4.2 m below the primary surface returns are caused by the optical reflections within the ATLAS receiver optical components, while the echoes from ~10 to ~45 m away from the primary surface signal are due to the PMT afterpulses with a longer time delay. The ICESat-2 ATLAS instrument response is derived from both a measurement of the transmitted laser pulse shape and measured photon events arising from land surfaces with different surface albedos. The ICESat-2 on-orbit measurements demonstrate that the ATLAS impulse response during different months and over different surface types is essentially identical.

## 1. Introduction

ICESat-2 is a follow-on mission to ICESat that provides global altimetry and atmospheric measurements with particular emphasis on surface elevation changes in the polar regions (Markus et al., 2017). The sole instrument aboard ICESat-2 is ATLAS, a green (532 nm) wavelength, photon-counting laser altimeter with a 10 kHz pulse repetition rate, and a footprint diameter of less than 17 m (Magruder et al., 2020; Magruder & Brunt, 2018; Markus et al., 2017). The ICESat-2 ATLAS measurement scenario is entirely different from both the full-waveform data collected by the avalanche photodiodes (APDs) used in the original ICESat mission (Abshire et al., 2005) and the low resolution surface elevation measurements acquired by CALIOP (i.e., the Cloud-Aerosol Lidar with Orthogonal Polarization), which uses PMTs in analog model (Hunt et al., 2009). The single-photon-sensitive detection technique used by ATLAS to measure photon time of flight provides the very high vertical resolution required to detect small temporal changes in polar ice elevations (Neumann et al., 2019; Popescu et al., 2018).

ATLAS uses PMTs as detectors to record the reflected photons. However, under certain conditions PMT measurements can be affected by various artifacts that can confound the interpretation of the signals and potentially lead to errors in subsequent analyses. For example, the transient response of the CALIOP PMTs is nonideal (Hu et al., 2007; Lu et al., 2013, 2014; 2018; Lu, Hu, Vaughan, et al., 2020; McGill et al., 2007). That is, following a strong backscattering signal, such as from the Earth's surface or a dense cloud, the signal initially falls off as expected but at some point begins decaying at a slower rate that is approximately exponential with respect to time (or distance). The CALIOP PMTs nonideal transient recovery can be seen over several hundreds of meters after a strong backscattering target (e.g., surface or water clouds), and thus make it wrongly appear as if the laser can penetrate the land surface to a depth of several hundreds of meters (Lu, Hu, Vaughan, et al., 2020; McGill et al., 2007). A second common PMT artifact is after pulsing, which is manifest as discrete, small amplitude signals that appear after onset of the main signal (Hamamatsu Photonics, 2006). Unlike the main signal, which is generated by some external light source, afterpulses are spurious signals generated internally by the PMTs themselves. As with the nonideal transient recovery of the CALIOP PMTs, PMT after-pulsing effects can yield misleading results when interpreting lidar measurements and thus should be removed whenever possible in order to obtain reliable data products.

PMT after-pulsing is not the only artifact that may be present in the ATLAS signals. Internal optical reflections in the receiver can result in some of the backscattered photons traveling slightly longer optical paths through the system. This longer path causes these photons to arrive at the detectors later than they otherwise should (Field et al., 2020). These "late" photons, which always appear some distance below a stronger initial pulse (e.g., due to land surface), are also called afterpulses in this paper. Based on pre-launch tests and optical ray trace predictions, Field et al., (2020) have identified the internal reflecting surfaces that generate optical path afterpulses in the ATLAS.

In this study, the ATLAS after-pulsing effects are characterized using ICESat-2 on-orbit measurements. Section 2 quantifies the behavior of the ATLAS afterpulses over land, ocean, sea ice, and land ice surfaces and summarizes the ATLAS detector's impulse response to date. The potential impacts of these after-pulsing effects on altimetry and ocean subsurface optical properties retrievals are discussed in Section 3. Some concluding remarks are given in Section 4.

## 2. ICESat-2 ATLAS Afterpulses

The analysis and results presented in this work use ICESat-2 geolocated photon data, contained in the ATL03 Release 003 data product, which are segmented into granules that span about 1/14th of an orbit and are stored as hdf5 files (Neumann et al., 2020). The ATL03 data provide latitude, longitude, and WGS-84 ellipsoidal height for all photons detected by ATLAS. Heights are corrected for several geophysical phenomena, such as effects of the atmosphere, tides, and solid Earth deformation (Neumann et al., 2018).

### 2.1. Afterpulses Seen in On-Orbit Measurements

Afterpulses are present in the ATLAS data stream regardless of the surface reflectance, but they are most easily seen and characterized after the strong signal returns measured from high reflectance surfaces above which there is minimal atmospheric attenuation. Figure 1 shows ICESat-2 photon heights from (a) land, (b) ocean, (c) sea ice, and (d) land ice surfaces along selected ICESat-2 ground tracks. The corresponding locations of these ground tracks are given in Figures S1 and S2. The blue dots in Figure 1 represent all photon events between likely background photon events and likely signal photon events, and the red dots indicate those signal photon events having high confidence levels. The high confidence photons are most likely backscattered from the Earth's surface.

Under ideal conditions, the lidar backscatter signal from a land surface rises almost instantaneously from a small value to a very large value and then decays rapidly and monotonically back to zero (Hunt et al., 2009). However, as shown in Figure 1a, in the ATLAS signals there are secondary echoes occurring down to ~45 m below the primary land surface return. Photon events at ~2.3 and ~4.2 m below the primary ocean surface return can be seen in Figure 1b. In Figure 1c, the afterpulses are seen at ~0.45, ~0.9, ~2.3, and ~4.2 m below the primary sea ice surface return. Figure 1d shows high confidence afterpulses occurring ~0.45 m below the surface of a melting pond over land ice. Figure S3 shows additional ATLAS measurements with

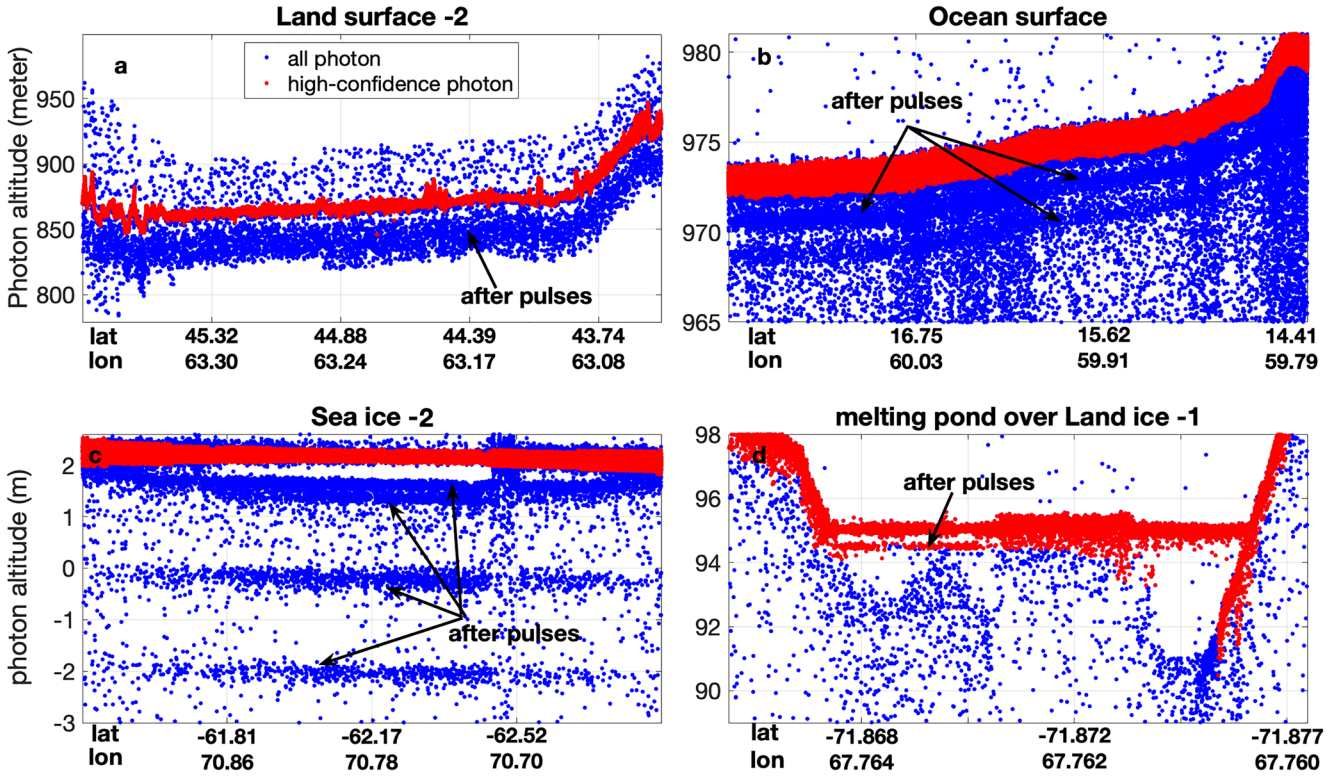


**Figure 1.** Geolocated photon heights (*y*-axis) along ICESat-2 ground tracks (*x*-axis) over (a) land, (b) ocean, (c) sea ice, and (d) melting ponds over land ice. The blue dots are photon events for all confidence levels and the red dots are photon events with high confidence levels. The afterpulses are easily seen beneath the primary surface returns. The corresponding ICESat-2 tracks are shown in Figures S1 and S2.

afterpulses occurring beneath sea ice surfaces. Compared with rough sea ice surfaces, where the time series of backscattered photons show no obvious horizontal structure below the ice surface, significant horizontal subsurface structure due to after-pulsing effects is clearly evident beneath smooth sea ice surfaces, as seen in Figure S3. The on-orbit measurements indicate that afterpulses are present in the ATLAS data acquired over land, ocean, sea ice, land ice and melting ponds and occur regardless of the surface type or reflectance.

### 2.2. Afterpulses Generation Mechanisms

ATLAS afterpulses arise from three distinct sources: ionization effects within the PMTs, internal optical reflections in the receiver, and detector saturation and dead-time recovery. To illustrate these different manifestations we choose nighttime measurements acquired over the Sahara Desert. These measurements are ideal for afterpulse studies because (a) nighttime data is not contaminated by solar background noise; (b) 532 nm laser light cannot penetrate the Sahara Desert so there are no subsurface photons in the backscattered signals; and (c) the lack of trees and other vegetation in the desert landscape largely eliminates delayed photon arrival effects.

We separate saturated and nonsaturated cases by using thresholds of 16 detected photons within 3 ns for the strong beams and 4 detected photons within 3 ns for the weak beams. For the strong beams, we selected those cases having between 3 and 8 surface photon counts to avoid relatively low or high surface photon numbers for nonsaturated cases. Figure S4 shows histograms of surface photon counts, which indicate that for most land surfaces, backscattered photon counts are less than 10 in nonsaturated cases. For nonsaturated cases having 3–8 surface photons within 3 ns, we are thus assured that there will be no PMT saturation effects (e.g., Figure 2a). Figure 2 shows the normalized land surface return over Sahara Desert for (a) nonsaturated and (b) saturated cases.

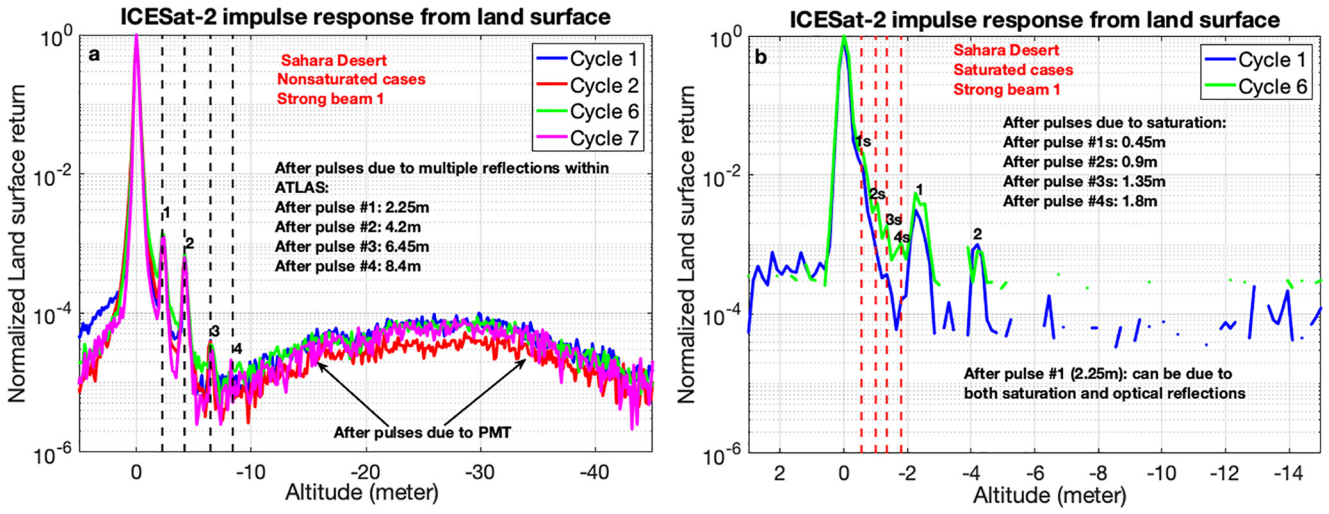


**Figure 2.** ICESat-2 ATLAS normalized land surface return over Sahara Desert (land #4 shown in Figure S1) for (a) nonsaturated cases and (b) saturated cases. The local surface elevation is set to 0 m, so that altitudes below the surface are expressed as negative values. The cycle numbers track the number of 91-day periods that have elapsed since ICESat-2 began science operations. The date for each cycle number is given in Table S1.

#### 2.2.1. Effect of PMT Afterpulses

There are two types of PMT afterpulses. One occurs after a very short delay (several nanoseconds to several tens of nanoseconds) following the primary signal pulse and the other appears with a longer delay ranging up to several microseconds. Afterpulses with the longer delay time are most likely caused by positive ions, which are generated by the ionization of residual gases in the photomultiplier tube. These positive ions return to the photocathode (ion feedback), producing multiple photoelectrons which result in afterpulses. Longer time delays with respect to the primary signal output pulse range from several hundred nanoseconds to over a few microseconds. PMT afterpulses with these longer time delays are typically seen from ~10 to ~45 m below the surface pulse. For example, while the PMT detector is not saturated (i.e., less than 16 returned surface photons for the strong beams), afterpulses can be clearly seen between ~10 and ~45 m below the land surfaces in Figures 1a and 2a. As indicated in Figure 2a, the amplitudes of these afterpulses are four orders of magnitude less than the amplitudes of the primary land return (Lu et al., 2019). As a result, if the signal contains subsurface photons (e.g., ocean or sea ice subsurface photons) or solar background noise during daytime, these afterpulses may not be readily apparent, because the amplitudes of the subsurface photons or background noise excursions can be higher than the PMT afterpulses. More details about the causes of PMT after pulsing can be found in the PMT handbook (Hamamatsu Photonics, 2006).

#### 2.2.2. Effect of Optical Reflections Within the ATLAS Receiver Optical Components

Within ATLAS receiver, there are two fibers transmitting ground return photons from the telescope to the detector (Martino et al., 2019). Fiber 1 has effective optical path length (EOPL) of ~4.2 m and fiber 2 has EOPL of ~2.25 m. Figure 2 in Field et al. (2020) shows the multiple paths within the ATLAS receiver that the returned photons can travel through in creating the surface return (first pulse) and several afterpulses. For clarity, Table 1 lists the afterpulses found in Figure 2a (dashed lines) from on-orbit measurements, which are due to effect of optical reflections within the ATLAS receiver optical components. These afterpulses captured from the flight data shown in Table 1 agree well with those obtained from pre-launch measurements (Field et al., 2020).

Afterpulses due to multiple reflections within ATLAS can be clearly seen at ~2.25, ~4.2, ~6.45, and ~8.4 m below land surfaces, as shown in Figure 2a. Summarizing the exposition in Field et al. (2020), the afterpulses at ~2.25, ~4.2, and ~6.45 m are caused by double reflections within the ATLAS receiver optical components and afterpulses at ~8.4 m are caused by quadruple reflections. Because 532 nm laser light can penetrate into lakes, oceans, sea ice, and land ice, subsurface backscatter will often obscure the afterpulses occurring at ~6.45 and ~8.4 m in measurements acquired over these surface types. Figure 1b shows photon events over ocean surface, where only the afterpulses at ~2.25 and ~4.2 m are visible. Moreover, daytime

**Table 1**
*Afterpulses Found From On-Orbit Measurements and Ordered by Depth*

| Afterpulses due to PMT saturation | | | |
|---|---|---|---|
| Afterpulses (AP) | Distance from land surface to afterpulses | Ratio of afterpulse to surface | Reasons |
| AP 1s | ~0.45 m | ~2e-2 | PMT saturation |
| AP 2s | ~0.9 m | ~4e-3 | PMT saturation |
| AP 3s | ~1.35 m | ~1.9e-3 | PMT saturation |
| AP 4s | ~1.8 m | ~1e-3 | PMT saturation |
| **Afterpulses due to multiple reflections within ATLAS system** | | | |
| Afterpulses (AP) # | Distance from land surface to afterpulses | Ratio of afterpulse to surface | Reason: Photons traveled extra times through the fibers due to reflections |
| AP 1 | 2.25 m (≈[a]EOPL of fiber 2) | ~1.5e-3 | Photons traveled through fiber 2 a total of 3 times |
| AP 2 | 4.2 m (≈EOPL of fiber 1) | ~7.2e-4 | Photons traveled through fiber 1 a total of 3 times |
| AP 3 | 6.45 m (≈EOPL of fiber 1+ EOPL of fiber 2) | ~3e-5–4e-5 | Photons traveled through both fibers a total of 3 times |
| AP 4 | 8.4 m (≈ 2 × EOPL of fiber 1) | ~1.7e-5 | Photons traveled through fiber 1 a total of 5 times. |
| Afterpulses caused by PMT ionization effects | | | |
| AP | ~10–45 m | ~ 1.3e-5–1e-4 | Caused by PMT ionization effects |

[a]EOPL: Effective Optical Path Length; fiber 1: EOPL ≈ 4.2 m, fiber 2: EOPL ≈ 2.25 m.

solar background noise can also be substantially higher than the afterpulses at ~6.45 and ~8.4 m. Consequently, afterpulses at ~6.45 and ~8.4 m below the surface are rarely, if ever, observed in daytime data.

### 2.2.3. Effect of the Dead-Time Circuit due to PMT Saturation

Figure 2b shows the saturated cases having surface photon counts greater than 16 for strong beam 1. The afterpulses appearing from ~0.45 to ~1.8 m after the first return peak are caused by effect of the dead-time circuit due to PMT saturation. Dead time is the recovery time required after an initial photon detection during which no new input photons can be counted. An illustration of dead-time effects is seen in the gap between the surface and subsurface photon events shown in Figures 1c and 1d. More specifically, ATLAS has a separate circuit for each PMT to generate a predictable and repeatable dead time of ~3 ns (Palm et al., 2018), corresponding to a distance of ~0.45 m between the primary and secondary echoes.

As seen in Figures 1c, 1d, and 2b, subsurface echoes separated by ~0.45 m are introduced by the dead-time circuit in response to PMT saturation. This occurs because smooth sea ice surfaces (e.g., Figures 1c or S3), flat water surfaces (e.g., Figure 1d) and desert surfaces (e.g., Figure 2b) have high reflectances that efficiently backscatter a large fraction of the incident light, so that photons are returned to the receiver at intervals much shorter than the 3 ns detector dead time. The ATLAS PMTs cannot correctly count all of the returning photons from these highly reflective surfaces; instead, the PMTs record returning photons spaced by integer multiples of the dead time, corresponding to the horizontal subsurface structures appearing at ~0.45, ~0.9, ~1.35, and ~1.8 m as seen in Figure 2b.

However, if the PMT does not saturate, dead time afterpulses will not appear. As seen in the nonsaturated cases shown in Figure 2a, there are no afterpulses from ~0.45 to ~1.8 m below land surface. But when measuring very strong signals, as indicated in Figures 1c, S3, 2b, the PMTs can be saturated multiple times. On the other hand, if there are subsurface photons or significant contributions from solar background noise, it can be difficult to correctly identify any dead time afterpulses that might normally appear at ~1.35 and ~1.8 m. This ambiguity arises because the signal magnitudes from subsurface photons or solar background noise can be greater than the magnitudes of the afterpulses at ~1.35 and ~1.8 m (e.g., see the results shown in Section 2.3).

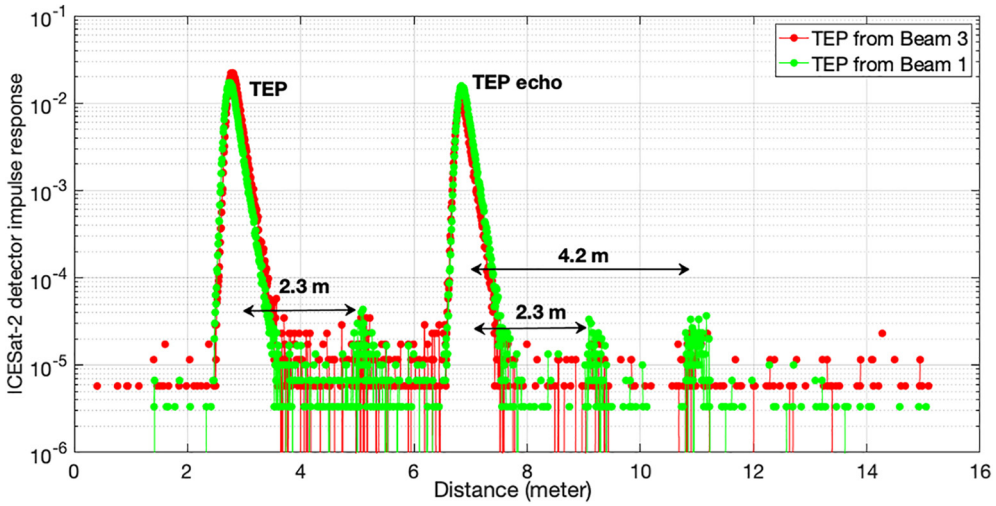


**Figure 3.** The shape of the TEP pulses as a function of time/distance from laser fire (Distance = light speed × time/2). The onset of the primary TEP pulse occurs at ~2.7 m while second large pulse is the TEP echo (Palm et al., 2018) generated by a reflection off the other end of the optical fiber. Data from beam 1 is shown in green. Data from beam 3 is shown in red.

### 2.3. ICESat-2 ATLAS Instrument Impulse Response

There are two ways to characterize the ATLAS detector's impulse response, which is defined as the aggregate temporal response of the ATLAS receiver optics and electronics to the backscattered photon arrival rate (Neuman et al., 2018). An estimate of the impulse response is derived from photon events recorded from the transmitter echo path (TEP). The ATLAS TEP is an optical path designed to allow some measure of timing and radiometric self-calibration on-orbit (Martino et al., 2018). The TEP takes a small fraction (~1 photon of every 10 to 20 laser shots) of the transmitted laser beam from the laser sampling assembly and feeds the light via fiber optics into an optical filter module. In this way, photons detected via the TEP traverse part of the transmit optical path, part of the receive optical path, and all of the receiver electronics that all other signal photons traverse (Neumann et al., 2018). Figure 3 shows the temporal distribution of transmitted photons via the TEP (referred to as the TEP pulse) as a function of laser transmit time from ATLAS beam 1 (green) and beam 3 (red). The primary TEP pulse arrives at ~2.7 m and the secondary TEP pulse (i.e., the TEP echo) arrives at ~6.8 m. The TEP echo is generated by a reflection off the other end of the optical fiber (Field et al., 2020). The afterpulses at ~2.3 and ~4.2 m after the TEP echo agree well with the afterpulses found in the measured photon events shown in Figures 1 and 2a.

The second method to characterize the ATLAS detector's impulse response is from the photons measured over land surfaces. More quantitatively, these photons are summed within 15 cm vertical bins over 10 consecutive laser pulses. Figure 4 shows the normalized signal intensity as a function of distance relative to the surface, where the surface altitudes are uniformly reindexed to zero meters. The black, blue, red, and pink curves are ATLAS detector's response during nighttime from land, ocean, rough sea ice and snow surfaces, respectively. For comparison, the ATLAS TEP echo pulse is shown in green in Figure 4. Moreover, Figure 4b also shows the ATLAS instrument responses for strong returns from smooth surfaces such as smooth sea ice (shown in red) during daytime and flat oceans (shown in blue) where the returns are due to specular reflection. The afterpulses in Figure 4b are easily seen at ~0.45, ~0.9, ~2.25, ~4.2, and 6.45 m. It can be seen from Figure 4 that the afterpulses from the measured photon events due to multiple reflections within ATLAS (~2.25 and ~4.2 m) completely agree with afterpulses from the TEP echo (green). As shown in Figure 4, the signals due to multiple reflections within ATLAS (e.g., at ~2.3 and ~4.2 m) are smaller than the primary surface return by more than two orders of magnitude, while the signal due to the PMT afterpulses with longer time delays (e.g., ~10–~45 m) is smaller than the primary surface return by ~4 orders of magnitude. Compared with the land surface response in black, the signal decay after the other surfaces is much slower. This is because 532 nm laser light can penetrate into ocean, sea ice and snow surfaces and hence there are

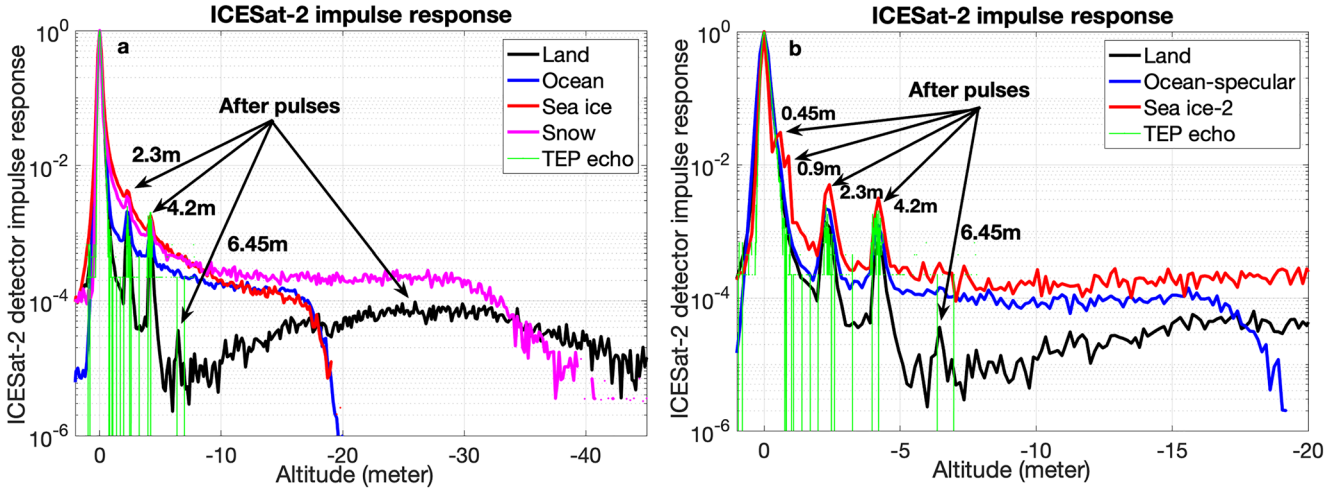


**Figure 4.** Quantitative illustration of the ICESat-2 ATLAS detector transient response from different surface types (different colors). The green curve is the TEP echo as shown in Figure 3. The peak at zero meters is the normalized signal from surface returns. Panel (a) shows results from rough surfaces during nighttime, while panel (b) also shows the instrument responses from strong smooth surfaces such as smooth sea ice (red) during daytime and flat oceans (blue). The surface elevation is set to 0 m, so that altitudes below the surface are given as negative values.

contributions from subsurface scattering, which are useful for investigating subsurface vertical structure using ICESat-2 measurements (Lu, Hu, Yang, et al., 2020).

Because the 532 nm laser pulse cannot penetrate the land surfaces (Hunt et al., 2009), the instrument response from land surface (black in Figure 4) accurately represents the ATLAS detector's impulse response (i.e., there are no photon contributions from subsurface scattering). The impulse responses from different land regions for six beams during different times are given in Figures 5 and 6. These data indicate that the ATLAS impulse response remains essentially constant, even when measured during different months and over varying land surface types having different surface albedos. Based on available ATL03 data to date, we do not expect significant changes in the ATLAS impulse response as a result of changes in transmitted pulse energy and/or land surface albedos.

## 3. Impact of ATLAS Afterpulses

### 3.1. After-Pulsing Effects on Altimetry

When plotted, the impact of ICESat-2 ATLAS afterpulses is usually visual, in that sequences of multiple echoes appear to occur at regular intervals below primary surface returns, as shown in Figure 1. Occasionally, photons due to after-pulsing effects can be mislabeled as surface photons, which can potentially affect the altimetry studies. Examples of these mislabeled photons are shown in Figures 1a and 1d, where some photons labeled as high confidence surface returns (red dots) are actually due to afterpulses. These mislabeled photons can be seen ~10 m below the land surface in Figure 1a. To mitigate this issue, several of the higher-level data products (e.g., ATL07 sea ice height) use a deconvolution approach to further refine the selection of surface photons and reject those photons that are most likely due to afterpulses or solar background during day time (Neumann et al., 2018). Characterizing the occurrence frequency and subsequent effects of these renegade photons is beyond the scope of this study. However, effective implementation of deconvolution algorithms requires accurate knowledge of the ATLAS instrument impulse response, which can be obtained from bare land surface returns (as shown in Figures 5 and 6) and TEP pulses (e.g., Figure 3).

### 3.2. After-Pulsing Effects on Ocean Subsurface

Compared with the land surface return (black line in Figure 4), the slower signal decay of the blue curve in Figure 4 indicates the prominent contributions from ocean subsurface signals. However, the ocean subsurface signal is contaminated by the afterpulses, which can be the same order of magnitude as the ocean

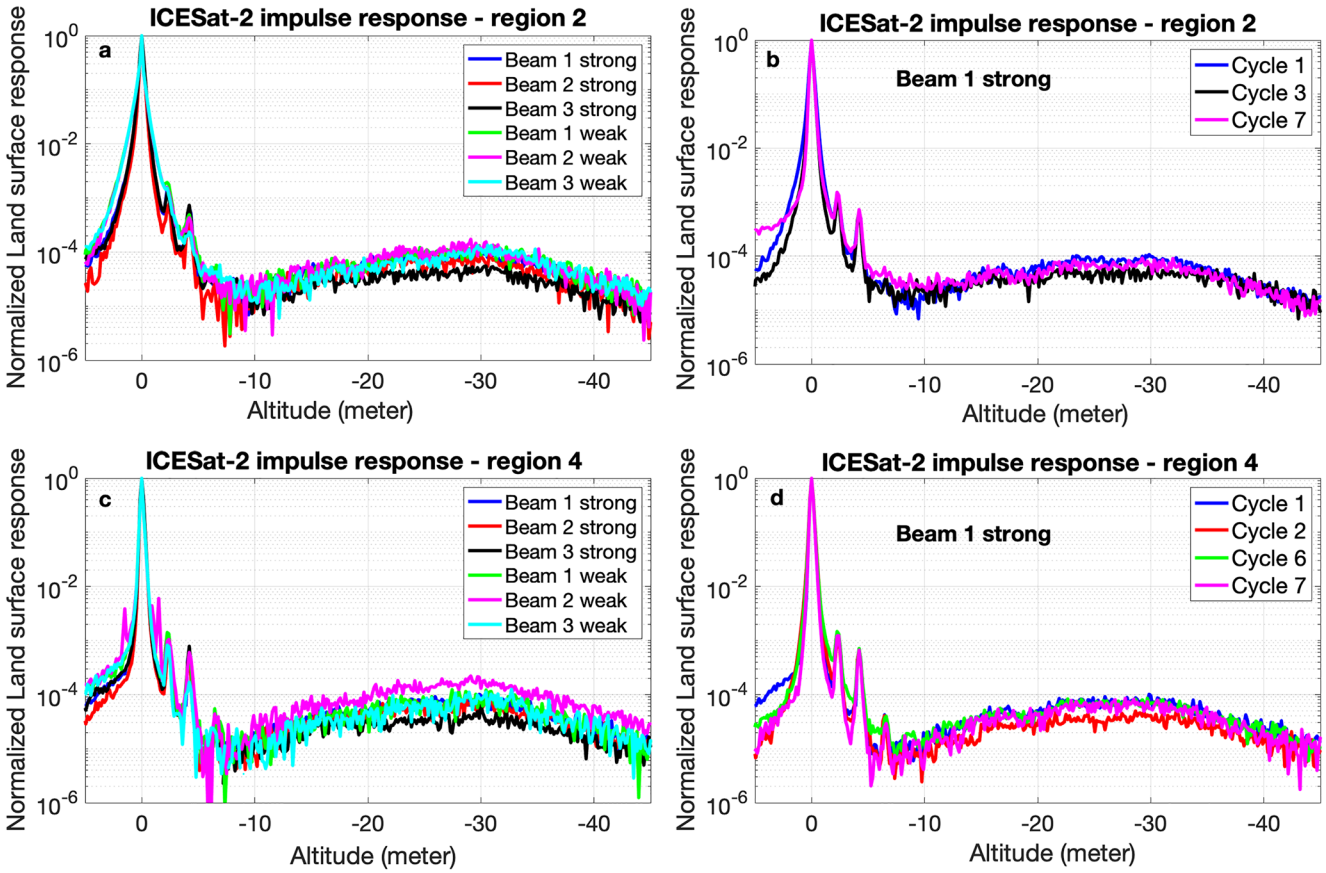


**Figure 5.** The ICESat-2 ATLAS impulse response from land surfaces for three strong and three weak beams over (a) land region 2 and (c) land region 4, and for different cycle numbers (b and d) corresponding to different dates as shown in Table S1. The studied land regions are shown in Figure S1.

subsurface signals, as indicated in Figures 4 and 7. Therefore, the ICESat-2 ATLAS after-pulsing effects must first be removed in order to obtain a reliable ocean subsurface profile. A deconvolution method described in (Lu et al., 2014; Lu, Hu, Vaughan, et al., 2020; Lu, Hu, Yang, et al., 2020) can be used to remove the ICESat-2 ATLAS afterpulses. As an illustration of the effectiveness of this deconvolution technique in removing ATLAS after-pulsing effects, Figure 7 shows an example of the ICESat-2 measured ocean subsurface signal (black) and its corresponding deconvolution (red). The prominent after pulsing artifacts seen in the measured signal have been completely eliminated in the deconvolved profile. A complete description of the approach can be found in Lu et al (2020).

## 4. Conclusions

We characterize the ICESat-2 ATLAS afterpulses and instrument impulse response using the on-orbit measurements. The afterpulses are typically present in the ICESat-2 measured photon events after almost any surface return, but are most easily seen beneath strong surface returns from highly reflective surfaces such as smooth sea ice. Three different types of afterpulses are found from on-orbit measurements: (a) afterpulses arising from ionization effects occurring within the ATLAS photomultiplier tubes (PMTs); (b) afterpulses caused by the detector dead-time circuit in response to PMT saturation; and (c) afterpulses caused by internal reflections within the optical components of the ATLAS receiver.

Afterpulses caused by PMT ionization effects can occur between ~10 to ~45 m below land surfaces. However, the presence of these PMT afterpulses may not be readily apparent when there is significant subsurface scattering or daytime solar background noise, because signal magnitudes from these sources can be greater than the afterpulse intensities. For example, in Figure 7 there are no obvious afterpulses visible at ~10 m

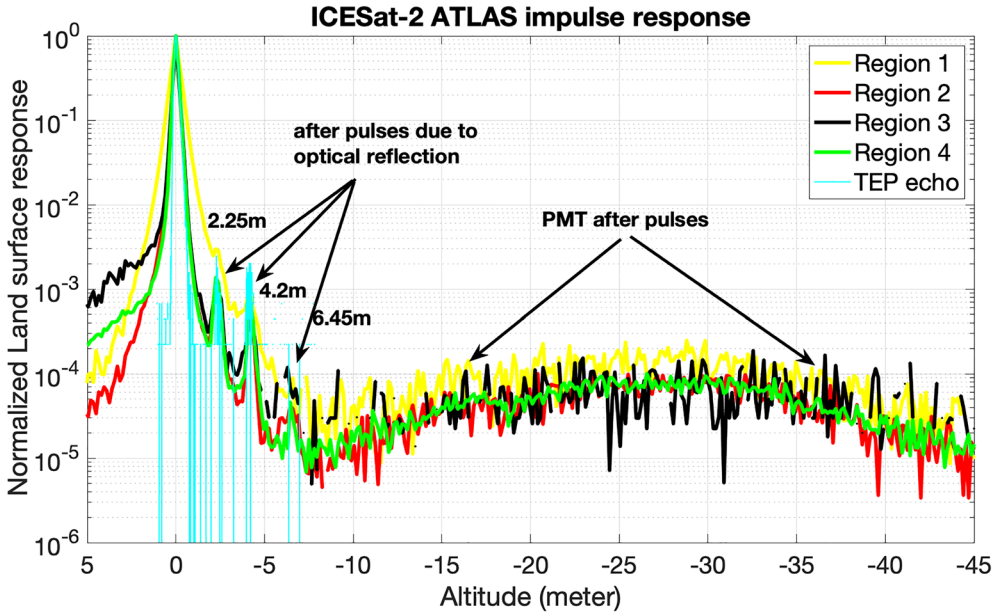


**Figure 6.** The ICESat-2 ATLAS impulse response for strong beam 1 over four studied land regions, with the different colors corresponding to the ground tracks shown in Figure S1. The cyan curve is the ICESat-2 impulse response from ATL03 directly. The land elevation is set to 0 m so that the altitudes below the land surface are all negative values. The wide pulse shown in yellow is due to vegetation effects.

below ocean surface because the subsurface signals are larger than the PMT afterpulses. As indicated in Figures 2a, 5 and 6, PMT afterpulses are ~4 orders of magnitude less than the peak surface signals.

Afterpulses caused by the dead-time circuit in response to PMT saturation can appear from ~0.45 to ~1.8 m following the first signal return peak. These dead-time afterpulses only occur when the detector has been saturated by an excess of backscattered photons. In this work we define saturation as photon arrival rates that are greater than ~16 within 3 ns for the strong beams or ~4 within 3 ns for the weak beams. As is the case with PMT afterpulses, the weaker dead-time afterpulses occurring at ~1.35 and ~1.8 m after an initial PMT saturation may not be visible when subsurface scattering or solar background noise is present (e.g., see the blue and red curves shown in Figure 4b).

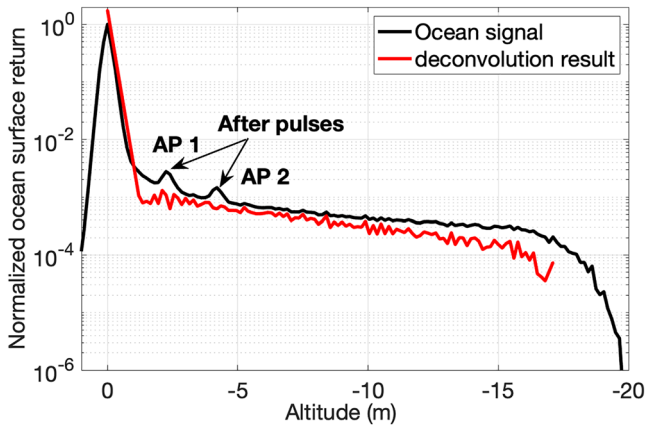


**Figure 7.** Vertical profiles of peak normalized ocean subsurface signals before (black) and after (red) application of the deconvolution method.

Afterpulses caused by the effect of optical reflections within the ATLAS receiver optical components can be visible at ~2.25, ~4.2, ~6.45, and ~8.4 m below land surfaces. Afterpulses at ~2.25, ~4.2, and ~6.45 m are caused by dual optical reflections within the optical components of the ATLAS receiver. The afterpulse at ~8.4 m is caused by quadruple reflections. The afterpulses at ~6.45 and ~8.4 m can be obscured by subsurface backscatter that can occur when 532 nm laser light penetrates into lakes, oceans, sea ice, or land ice surfaces. Figure 7 shows examples of ocean surface and subsurface signals, which indicates only the afterpulses at ~2.25 and ~4.2 m are visible. Moreover, during daytime, the solar background noise can also be higher than the optical reflections afterpulses at ~6.45 and ~8.4 m, and thus render them effectively invisible.

The ICESat-2 on-orbit measurements demonstrate that the ATLAS instrument impulse response remain essentially identical when evaluated for different months and over different surface types. An accurate characterization of the ICESat-2 ATLAS impulse response can be obtained by aggregating land surface returns, as shown in Figures 5 and 6. An accurate representation of the impulse response is essential for subsequent

application of the deconvolution methods used to generate ICESat-2 higher-level data products (e.g., ATL07, ATL12, and ATL13) and for ocean subsurface optical properties retrieval in order to remove the ICESat-2 ATLAS after-pulsing effects.

## Conflict of Interests

The authors declare no conflicts of interest relevant to this study.

## Data Availability Statement

The ICESat-2 data are publicly available through the National Snow and Ice Data Center (NSIDC). The geolocated photon data (ATL03) are found online (https://nsidc.org/data/atl03). Datasets for this research are available in these in-text data citation references: Neumann et al. (2020).

**Acknowledgments**
The authors would like to thank the NASA ICESat-2 team for providing the data used in this study. We thank Tom Neumann, Anthony Martino, Christopher Field and an anonymous reviewer for constructive comments and advice that helped to considerably improve this work. Funding for the lead author was provided by the NASA award (grant numbers 80NSSC20K0129).

## References

Abshire, J. B., Sun, X., Riris, H., Sirota, J. M., McGarry, J. F., Palm, S., et al. (2005). Geoscience Laser Altimeter System (GLAS) on the ICESat Mission: On-orbit measurement performance. *Geophysical Research Letters*, *32*(21), L21S02. https://doi.org/10.1029/2005gl024028

Field, C., Martino, A., & Ramos-Izquierdo, L. (2020). *ICESat-2/ATLAS instrument linear system impulse response*. https://doi.org/10.1002/essoar.10504651.1

Hamamatsu Photonics (2006). Chapter 4 Characteristics of photomultiplier tubes. In Photomultiplier tubes basics and applications (3rd ed.).

Hu, Y., Powell, K., Vaughan, M., Tepte, C., Weimer, C., Beherenfeld, M., et al. (2007). Elevation information in tail (EIT) technique for lidar altimetry. *Optics Express*, *15*(22), 14504–14515. https://doi.org/10.1364/OE.15.014504

Hunt, W. H., Winker, D. M., Vaughan, M. A., Powell, K. A., Lucker, P. L., & Weimer, C. (2009). CALIPSO lidar description and performance assessment. *Journal of Atmospheric and Oceanic Technology*, *26*(7), 1214–1228. https://doi.org/10.1175/2009JTECHA1223.1

Lu, X., Hu, Y., Liu, Z., Zeng, S., & Trepte, C. (2013). CALIOP receiver transient response study. *Proceedings of SPIE 8873, Polarization Science and Remote Sensing VI*, *8873*, 887316. https://doi.org/10.1117/12.2033589

Lu, X., Hu, Y., Trepte, C., Zeng, S., & Churnside, J. H. (2014). Ocean subsurface studies with the CALIPSO spaceborne lidar. *Journal of Geophysics Research: Oceans*, *119*(7), 4305–4317. https://doi.org/10.1002/2014jc009970

Lu, X., Hu, Y., Vaughan, M., Rodier, S., Trepte, C., Lucker, P., & Omar, A. (2020). New attenuated backscatter profile by removing the CALIOP receiver's transient response. *Journal of Quantitative Spectroscopy and Radiative Transfer*, *255*, 107244. https://doi.org/10.1016/j.jqsrt.2020.107244

Lu, X., Hu, Y., & Yang, Y. (2019). Ocean Subsurface Study from ICESat-2 Mission. In *2019 photonics & electromagnetics research symposium - fall (PIERS - fall)* (pp. 910–918). https://doi.org/10.1109/PIERS-Fall48861.2019.9021802

Lu, X., Hu, Y., Yang, Y., Bontempi, P., Omar, A., & Baize, R. (2020). Antarctic spring ice-edge blooms observed from space by ICESat-2. *Remote Sensing of Environment*, *245*, 111827. https://doi.org/10.1016/j.rse.2020.111827

Lu, X., Hu, Y., Yang, Y., Vaughan, M., Liu, Z., Rodier, S., et al. (2018). Laser pulse bidirectional reflectance from CALIPSO mission. *Atmosphere Measure Techniques*, *11*(6), 3281–3296. https://doi.org/10.5194/amt-11-3281-2018

Magruder, L. A., & Brunt, K. M. (2018). Performance analysis of airborne photon- counting lidar data in preparation for the icesat-2 mission. *IEEE Transactions on Geoscience and Remote Sensing*, *56*(5), 2911–2918. https://doi.org/10.1109/TGRS.2017.2786659

Magruder, L. A., Brunt, K. M., & Alonzo, M. (2020). Early ICESat-2 on-orbit geolocation validation using ground-based corner cube retro-reflectors. *Remote Sensing*, *12*, 3653. https://doi.org/10.3390/rs12213653

Markus, T., Neumann, T., Martino, A., Abdalati, W., Brunt, K., Csatho, B., et al. (2017). The Ice, Cloud, and land Elevation Satellite-2 (ICESat-2): Science requirements, concept, and implementation. *Remote Sensing of Environment*, *190*, 260–273. https://doi.org/10.1016/j.rse.2016.12.029

Martino, A. J., Bock, M. R., Jones, R. L., III, Neumann, T. A., Hancock, D. W., III, Dabney, P. W., & Webb, C. E. (2018). *ICE, CLOUD, and land elevation satellite (ICESat-2) project: Algorithm theoretical basis document (ATBD) for ATL02 (Level-1B) data product processing*. Greenbelt, Maryland: NASA Goddard Space Flight Center. https://doi.org/10.5067/9GED1JJV41C0

Martino, A. J., Neumann, T. A., Kurtz, N. T., & McLennan, D. (2019). ICESat-2 mission overview and early performance. *Proceedings of SPIE, 11151, Sensors, Systems, and Next-Generation Satellites, XXIII*, 111510C. https://doi.org/10.1117/12.2534938

McGill, M. J., Vaughan, M. A., Trepte, C. R., Hart, W. D., Hlavka, D. L., Winker, D. M., & Kuehn, R. (2007). Airborne validation of spatial properties measured by the CALIPSO lidar. *Journal of Geophysical Research*, *112*(D20), D20201. https://doi.org/10.1029/2007jd008768

Neumann, T., Brenner, A., Hancock, D., Robbins, J., Saba, J., & Harbeck, K. (2018). *ICE, CLOUD, and land elevation satellite - 2 (ICESat-2) project algorithm theoretical basis document (ATBD) for global geolocated photons ATL03*. Greenbelt, Maryland: NASA Goddard Space Flight Center. https://doi.org/10.5067/T0HGP0893I9R

Neumann, T. A., Brenner, A., Hancock, D., Robbins, J., Saba, J., Harbeck, K., et al. (2020). *ATLAS/ICESat-2 L2A Global Geolocated Photon Data, Version 3*. Boulder, CO:NASA National Snow and Ice Data Center Distributed Active Archive Center. https://doi.org/10.5067/ATLAS/ATL03.003

Neumann, T. A., Martino, A. J., Markus, T., Bae, S., Bock, M. R., Brenner, A. C., et al. (2019). The Ice, Cloud, and Land Elevation Satellite - 2 mission: A global geolocated photon product derived from the Advanced Topographic Laser Altimeter System. *Remote Sensing of Environment*, *233*, 111325. https://doi.org/10.1016/j.rse.2019.111325

Palm, S., Yang, Y., & Herzfeld, U. (2018). *ICESat-2 Algorithm Theoretical Basis Document for the Atmosphere, Part 1: Level 2 and 3 Data Products, Version 7.5*. https://doi.org/10.5067/X6N528CVA8S9

Popescu, S. C., Zhou, T., Nelson, R., Neuenschwander, A., Sheridan, R., Narine, L., & Walsh, K. M. (2018). Photon counting LiDAR: An adaptive ground and canopy height retrieval algorithm for ICESat-2 data. *Remote Sensing of Environment*, *208*, 154–170. https://doi.org/10.1016/j.rse.2018.02.019